Atmos. Meas. Tech. Discuss., 3, 2535–2577, 2010
www.atmos-meas-tech-discuss.net/3/2535/2010/
doi:10.5194/amtd-3-2535-2010


Atmospheric Measurement Techniques Discussions



# Prediction of rainfall measurement errors using commercial microwave communication links

**A. Zinevich**[1], **H. Messer**[2], **and P. Alpert**[3]

[1]The Porter School of Environmental Studies, Tel Aviv University, Israel
[2]School of Electrical Engineering, Tel Aviv University, Israel
[3]Department of Geophysics and Planetary Sciences, Tel Aviv University, Israel

Received: 1 March 2010 – Accepted: 17 May 2010 – Published: 4 June 2010

Correspondence to: A. Zinevich (artemsin@post.tau.ac.il)

Published by Copernicus Publications on behalf of the European Geosciences Union.







## Abstract

Commercial microwave radio links forming cellular communication networks are known to be a valuable instrument for measuring near-surface rainfall. However, operational communication links are more uncertain relatively to the dedicated installations since their geometry and frequencies are optimized for high communication performance rather than observing rainfall. Quantification of the uncertainties for measurements that are non-optimal in the first place is essential to assure usability of the data.

In this work we address modeling of environmental impairments, i.e. variability of drop size distribution along a link and spatial variability of rainfall in the link's neighborhood, as well as instrumental ones, i.e. signal variability due to antenna wetting, baseline attenuation uncertainty and digital quantization. Expressions for root mean squared error (RMSE) for estimates of path-averaged and point rainfall have been derived. To verify the RMSE expressions quantitatively, path-averaged measurements from 23 operational communication links have been compared to records of five nearby rain gauges over three rainstorm events. It has been demonstrated that the major sources of link-gauge discrepancies are spatial variability and baseline attenuation uncertainty; the former remains important for up to 120 min temporally averaged measurements. The experiments show that the predicted RMSE on the average fit the measured RMSE for various link lengths, rain rates and temporal intervals; above 90% of experimental errors for 1–60 min averages and 88% for 120 min are explained by the model. In addition, the dependence of the optimal coefficients of a conventional wet antenna attenuation model on spatial rainfall variability has been shown.

The expressions for RMSE of the path-averaged rainfall estimates can be useful for integration of measurements from multiple heterogeneous links into data assimilation algorithms.





AMTD
3, 2535–2577, 2010



## 1 Introduction

Electromagnetic waves, especially at high (tens of GHz) radio frequencies are known to be affected by atmospheric conditions in general and by precipitation in particular. The specific rainfall-induced attenuation $K$ [dB km$^{-1}$] of a radio signal at the frequencies of tens of GHz is dominated by the effects of rainfall $R$ [mm h$^{-1}$] and is governed by a well-known power law equation

$$K = aR^b \tag{1}$$

where the parameters $a$ and $b$ are, in general, functions of link frequency, polarization and drop size distribution (DSD) (Jameson, 1991). Rainfall estimation using microwave links has been studied over the last few decades (for example, Atlas and Ulbrich, 1977; an overview can be found in Zinevich et al., 2009), but only recently (Messer et al., 2006; Leijnse et al., 2007a) it has been demonstrated that data recorded in commercial cellular communication networks can be used to estimate space-time rainfall intensities.

Microwave links, being an indirect rainfall measurement tool, suffer from inherent inaccuracies. It was shown (Atlas and Ulbrich, 1977) that at the frequencies of about 35 GHz, the power-law relationship is approximately linear and is essentially independent of DSD and temperature, showing empirical errors of less than 10%. However, the uncertainties in determination of path-averaged rainfall intensity due to variation in DSD increase with lowering frequency to 9 GHz to more than 20%. Rincon and Lang (2002) have shown that the instantaneous estimates based on power law equation (Eq. 1) tend to overestimate the actual rainfall, especially at high rain rates where variations in DSD affect the power law measurements, even though the agreement between power law and dual frequency estimates is very good during the intervals of stratiform rain. Wet antenna attenuation has been found to have great impact on measurement accuracy (Minda and Nakamura, 2005) if this effect is not taken into account. The uncertainties in determination of clear air attenuation due to water vapor and scintillation effects also have a direct impact on measurement quality (Holt et al.,





AMTD
3, 2535–2577, 2010



2003; Rahimi et al., 2003; David et al., 2009). The effects of raindrop canting angles, temperature, intra- and inter-storm variations of rainfall microstructure, link length and frequency, temporal sampling strategy, power resolution and wetting of antennas have been addressed by Aydin and Daisley (2002), Berne and Uijlenhoet (2007), Leijnse et al. (2007b, 2008a, b).

However, the latter studies on uncertainties have been oriented toward estimation of expected errors using a simulation framework, primarily to choose the optimal conditions for measurement of path-averaged rainfall. The simulation results represent climatological average estimates of uncertainty that do not account for inter- and intra-storm variation of rainfall intensity. The results are therefore not directly applicable for accurate on-line variance estimation that is required, for example, for assimilation of microwave rainfall measurements (Grum et al., 2005; Zinevich et al., 2009). The experimental verification of the accuracy of uncertainty quantification has received little attention by now; it has been shown by Leijnse et al. (2008a) that experimentally measured errors considerably exceed the predicted ones, since not all error sources have been taken into account.

On the other hand, commercial hardware installations are characterized by lack of control over link parameters. The links are installed in the way that maximizes communication performance rather than the accuracy of rainfall measurements; having online variance estimation is essential for accurate integration of observations from multiple links.

This work attempts to build a framework for quantitative estimation of uncertainties of path-averaged microwave rainfall measurements. The expressions for root mean squared error (RMSE) $E[ee]$ of the estimation error $e = R - \hat{R}$ for estimates $\hat{R}$ of path-averaged rainfall $R$ have been derived. The RMSE estimates take into account the major error sources: DSD variations along a link and signal variations due to antenna wetting, quantization of the signal attenuation measurements and uncertainty in the determination of the baseline (zero rainfall) attenuation. A model of rainfall spatial variation is adopted to facilitate comparison of path-averaged rainfall estimates with





AMTD
3, 2535–2577, 2010



nearby rain gauges, still the most reliable instrument for surface rainfall measurements.

The paper is organized as follows: in Sect. 2 a model for mean squared error (MSE) of path-averaged rainfall estimation error is formulated. The calibration of model parameters is addressed in Sect. 3. The spatial rainfall variability model is described in Sect. 4. Experimental errors and predicted RMSE are studied by comparing link and gauge observations in Sect. 5. Section 6 concludes the manuscript.

## 2 Uncertainty models

A simplified model for microwave attenuation $A_M$, measured by a radio receiver is

$$A_M = A_0 + A_R + A_w + n_q \quad (2)$$

where $A_0$ is baseline (dry air) attenuation, $A_R$ is path-integrated rainfall-induced attenuation, $A_w$ is excess attenuation due to wet antenna and $n_q$ is observation quantization noise, modeled as a uniformly distributed random variable (Widrow and Kollár, 2008) with variance

$$\sigma_q^2 = \frac{\Delta^2}{12} \quad (3)$$

for $\Delta$ dB quantization interval. Equation (3) can be assumed valid for signals $A_R$, $A_w$ with dispersion much higher than $\Delta$; note that this assumption does not hold for weak rainfall. Both $A_R$ and $A_w$ depend on DSD distribution along a link; besides, all components are independent.

### 2.1 Uncertainties due to DSD variations

The path-integrated rainfall-induced attenuation $A_R$ results from absorption and scattering of electromagnetic waves by raindrops, distributed at a point $x$ along the $L$ km





AMTD
3, 2535–2577, 2010



link as $N_d(D,x)$, where $D$ is the equivolumetric raindrop diameter and $Q_d(D)$ is the extinction cross-section at given frequency and polarization (Atlas and Ulbrich, 1977):

$$A_R = 0.4343 \int_L dx \left( \int_D dD N_d(D,x) Q_d(D) \right)$$
$$= 0.4343 \int_D dD \bar{N}_d(D,L) Q_d(D) \quad (4)$$

where $\bar{N}_d(D,L) = \int_L N_d(D,x)dx$ is the path-integrated DSD. Similarly, the path-averaged rainfall $R_L$ is given by

$$R_L = \frac{0.6\pi}{L} \int_D dD \bar{N}_d(D,L) V_d(D) D^3, \quad (5)$$

where $V_d(D)$ is the raindrop terminal velocity. Since both $V_d(D)$ and the Rayleigh scattering cross-section can be approximated by power laws $V_d(D) = 3.78D^{0.67}$, $Q_d(D) = CD^n$ (Atlas and Ulbrich, 1977), both $A_R$ and $R_L$ can be considered higher-order moments of the DSD $N_d(D)$. The relation between $A_R$ and $R_L$ becomes linear at frequencies of about 34 GHz where the power $n$ in the cross-section expression equals to that of $V_d(D)$. Commercial microwave links operate at various frequencies; uncertainty in determination of path-averaged rain rate from attenuation measurements increases as frequency lowers (Atlas and Ulbrich, 1977).

For a given link, the stochastic relationship between $A_R$ and $R_L$ can be obtained empirically by fitting their estimates based on the DSD measurements of $\bar{N}_d(D,L)$ for a given link length $L$. For convenience, let us write an expression for the expected value of $R_L$ given $A_R$ according to Eq. (1) with inverted power law coefficients $\beta = b^{-1}$, $\alpha = (aL)^{-\beta}$:

$$\hat{R}_L(A_R) = E\left[R_L | A_R\right] \cong \alpha A_R^{\beta}. \quad (6)$$





AMTD
3, 2535–2577, 2010



The MSE of $R_L$ due to DSD variations can be modeled using another ad hoc power-law expression with two link-specific parameters $\gamma, \delta$ (we adopt a notation $\sigma^2(R|A) = E\left[\left(R - \hat{R}(A)\right)^2 | A\right]$ for MSE):

$$\hat{\sigma}^2_{\mathrm{DSD}}(R_L|A_{\mathrm{R}}) = E\left[\left(R_L - \hat{R}_L(A_{\mathrm{R}})\right)^2 | A_{\mathrm{R}}\right] \cong \gamma A_{\mathrm{R}}^{\delta}. \quad (7)$$

The verification of adequacy of the power law parametric form is addressed in the context of a model, comprising wet attenuation effects, in Sect. 3, *c*.

## 2.2 Uncertainties due to antenna wetting

A thin film of water on an antenna or a radome is known to cause a considerable attenuation of the received signal. A simplified empirical two-parameter model for a wet antenna attenuation estimate $\hat{A}_{\mathrm{w}}$, originating from Kharadly and Ross (2001) have been used by Minda and Nakamura (2005), Leijnse et al. (2007b), Zinevich et al. (2009):

$$\hat{A}_{\mathrm{w}} = c_1\left(1 - e^{-c_2(A_{\mathrm{R}} + A_{\mathrm{w}})}\right), \quad (8)$$

Denoting $a_{\mathrm{w}}(A) = c_1\left(1 - e^{-c_2 A}\right)$, let us represent the true wet antenna attenuation as

$$A_{\mathrm{w}} = a_{\mathrm{w}}(A_{\mathrm{R}} + A_{\mathrm{w}}) + n_{\mathrm{w}} \quad (9)$$

where $n_{\mathrm{w}}$ is noise, caused by rainfall variations near the antennas. Substituting unknown $A_{\mathrm{R}} + A_{\mathrm{w}}$ from Eq. (2) into Eq. (8), Eq. (2) transforms into

$$A_{\mathrm{R}} + n_{\mathrm{w}} = A_{\mathrm{M}} - A_0 - n_{\mathrm{q}} - a_{\mathrm{w}}\left(A_{\mathrm{M}} - A_0 - n_{\mathrm{q}}\right). \quad (10)$$

Since both $n_{\mathrm{w}}$ and the measurement error in $R_L$ are caused by DSD variability along a link, they should be modeled jointly using the same DSD data. Taking into account that the effect of $n_{\mathrm{w}}$ on rainfall estimate decreases with increase of $A_{\mathrm{R}} + n_{\mathrm{w}}$ according





AMTD
3, 2535–2577, 2010



to Eq. (8) (for large $A_M$, $A_w \to c_1$ and is weakly affected by its variations), a following ad hoc parametric MSE model is proposed:

$$\hat{\sigma}^2_{DSD+Wet}(R_L|A_R+n_w) = E\left[\left(R_L - \hat{R}_L(A_R+n_w)\right)^2 | A_R+n_w\right] \cong \gamma(A_R+n_w)^\delta e^{-\varepsilon(A_R+n_w)}. \quad (11)$$

The model given by Eq. (6) can be adopted for $\hat{R}_L(A_R+n_w)$ keeping in mind that even zero-mean $n_w$ leads to a biased estimate of $R_L$ since

$$E\left[\alpha(A_R+n_w)^\beta\right] \neq E\left[\alpha A_R^\beta\right] \quad (12)$$

due to non-linearity of the power law Eq. (6).

### 2.3 Uncertainties due to baseline variation

The level of baseline (dry) attenuation $A_0(t)$, where $t$ is a time index, varies in time due to primarily variations of water vapor concentration in the atmosphere, ducting and scintillation; its estimation is complicated by signal quantization. The baseline attenuation estimates are calculated as sample mean ($\hat{A}_{0-}$,$\hat{A}_{0+}$) of attenuation measurements immediately before and after a rainstorm, detected according to nearby rain gauges; for a practical applications, existing dry/rainy interval detection techniques can be used (Rahimi et al., 2003; Upton et al., 2005; Goldshtein et al., 2009). A smooth instantaneous estimate $\hat{A}_0(t)$ is then obtained by cubic spline interpolation between $\hat{A}_{0\pm}$; slowly changing trends of $A_0$ with periods of a few hours to days, attributed to humidity variations, are compensated in this way. The noise $n_0$ due to short-time variations

$$n_0(t) = A_0(t) - \hat{A}_0(t) \quad (13)$$

is zero mean under an assumption that interpolation adequately describes the long-term baseline changes.





AMTD
3, 2535–2577, 2010



To quantify uncertainty of $\hat{A}_{0\pm}$ (MSE of $n_0$), sample MSE $\hat{\sigma}^2_{0\pm}$ have been calculated over dry intervals, assuming that short-term baseline variations during dry and rainy periods have similar statistical properties. Measurement of temporally averaged rainfall requires estimation of baseline variability in the same temporal scale. To facilitate estimation of accumulated raifnall amounts over an interval of $\Delta t$ samples length, the dry attenuation measurements have been averaged over a sliding window of length $\Delta t$ prior to calculation of $\hat{\sigma}^2_{0\pm}$ (note that averaging of rain rates is not equal to averaging attenuations, due to non-linearity of Eq. (1); these differences are of second order and are neglected for MSE prediction).

In some cases, the natural short-term variations in $A_0$ due to the atmospheric scintillation produce a dithering effect on the quantized signal so that sample mean represents the average baseline attenuation; for short $\Delta t$, quantization noise in dry samples is also absorbed into $\hat{\sigma}^2_{0\pm}$ that may lead to overestimation of baseline variability. For short links or at low frequencies, the natural fluctuations of the base level attenuation are comparable in magnitude to the quantization interval $\Delta$=1 dB (in the present study). In this case, quantization causes a nonlinear distortion of the signal; the true $A_0$ is known to within $\Delta$. Increasing sample size does not decrease the variance of quantization error, given by Eq. (3), and the estimation of true $\hat{\sigma}^2_{0\pm}$ is complicated. A possible heuristics in this case is to limit $\hat{\sigma}^2_{0\pm}$ to the minimum given by Eq. (3), supposing that near-zero $\hat{\sigma}^2_{0\pm}$ indicates that the nonlinear quantization effect dominates other variability sources. Similarly to $\hat{A}_0(t)$, the instantaneous estimates of $\hat{\sigma}^2_0(t)$ are obtained by cubic spline interpolation of $\hat{\sigma}^2_{0\pm}$ (Fig. 1). Because of non-linear quantization effects, the process $\hat{A}_0(t)$ is, in general, non-ergodic; quantization error in baseline estimate may affect an entire rain event, introducing a bias in estimation of path-averaged rainfall.

Substituting Eq. (13) into Eq. (10), we get the signal distortion model

$$A_R + n_w = A_M - \hat{A}_0 - n_0 - n_q - a_w\left(A_M - \hat{A}_0 - n_0 - n_q\right). \quad (14)$$





AMTD
3, 2535–2577, 2010



According to Eq. (14), one can see that $n_q$ can be assumed zero-mean: regardless of how quantization is performed (rounding, flooring or ceiling), the possible bias due to quantization presents in both the baseline $\hat{A}_0$ and the measurement $A_M$ and is cancelled for $A_M - \hat{A}_0$.

### 2.4 Uncertainties of estimation of path-averaged rainfall

Using a linear approximation of Eq. (14) around $A_M - \hat{A}_0$, we can rewrite it as

$$\hat{A}_w\left(A_M - \hat{A}_0 - n_q - n_0\right) \cong a_w\left(A_M - \hat{A}_0\right) + a'_w\left(A_M - \hat{A}_0\right)\left(-n_q - n_0\right), \quad (15)$$

$$A_R + n_w \cong A_M - \hat{A}_0 - a_w\left(A_M - \hat{A}_0\right) - t_M \cdot \left(n_q + n_0\right), \quad (16)$$

where $a'_w$ is the first derivative of $a_w$ w.r.t. $A_M - \hat{A}_0$, and $t_M = \left(1 - c_1 c_2 \exp\left(-c_2\left(A_M - \hat{A}_0\right)\right)\right)$ is an auxiliary variable. Neglecting the errors of linear approximation, recalling that both $n_q$ and $n_0$ are zero-mean and independent, the estimates of the rainfall-induced attenuation $\hat{A}_R = E\left[A_R + n_w \middle| A_M - \hat{A}_0\right]$ and its MSE become

$$\hat{A}_R = A_M - \hat{A}_0 - a_w\left(A_M - \hat{A}_0\right), \quad (17)$$

$$\hat{\sigma}^2\left[A_R + n_w \middle| A_M - \hat{A}_0\right] \cong t_M^2\left(\frac{\Delta^2}{12} + \sigma_0^2\right). \quad (18)$$

Substituting Eq. (17) into Eq. (16) and substituting $A_R + n_w$ for $A_R$ in Eq. (6), we can rewrite the latter as

$$\hat{R}_L\left(\hat{A}_R\right) = E\left[\alpha(A_R + n_w)^\beta \middle| \hat{A}_R\right] \cong E\left[\alpha\left(\hat{A}_R - t_M\left(n_q + n_0\right)\right)^\beta\right]. \quad (19)$$





AMTD
3, 2535–2577, 2010



Again, using a linear approximation around $\hat{A}_R$, denoting another auxiliary variable $d_M = \alpha\beta\hat{A}_R^{\beta-1} t_M$, the Eq. (19) simplifies to a trivial

$$\hat{R}_L\left(\hat{A}_R\right) \cong E\left[\alpha\hat{A}_R^{\beta} - d_M\left(n_q + n_0\right)\right] = \alpha\hat{A}_R^{\beta}. \quad (20)$$

Similarly, noticing independence of $n_q$ and $n_0$ with DSD-related uncertainties and substituting the Eq. (11), Eq. (18) transforms into

$$\hat{\sigma}^2\left[R_L \middle| \hat{A}_R\right] \cong E\left[\left(R - \alpha\hat{A}_R^{\beta} + d_M\left(n_q + n_0\right)\right)^2\right]$$
$$\cong \hat{\sigma}^2_{\mathrm{DSD+Wet}}\left(R_L \middle| \hat{A}_R\right) + d_M^2\left(\frac{\Delta^2}{12} + \hat{\sigma}_0^2\right). \quad (21)$$

### 2.5 Temporal averaging

To get a better insight into the effect of various error sources as a function of temporal averaging intervals, let us estimate the MSE of path- and time-averaged rain rate $\langle R_L(t)\rangle$ over $\Delta t$ minute interval, $t = 1\ldots\Delta t$, given a set of instantaneous attenuation measurements $\Omega = \{A_M(t) - \hat{A}_0(t);\ t = 1,\ldots,\Delta t\}$. By substituting the averaging operator $\langle\cdot\rangle$ into Eq. (11),

$$\hat{\sigma}^2\left[\langle R_L(t)\rangle|\Omega\right] \cong E\left[\left(\langle R_L(t)\rangle - \left\langle\alpha\hat{A}_R(t)^{\beta} + d_M(t)\left(n_q(t) + n_0\right)\right\rangle\right)^2\right]. \quad (22)$$

Here, $d_M(t)$ is obtained from $d_M$ by substituting $\hat{A}_R(t)$, $A_M(t)$, $\hat{A}_0(t)$ for $\hat{A}_R$, $A_M$, $\hat{A}_0$. Note that $n_0$ does not depend on $t = 1\ldots\Delta t$ (that is, the typical period of variations of $n_0$ is assumed to be much longer than $\Delta t$; Eq. (22) does not account for instantaneous baseline variations due to scintillation since their effect on $\langle R_L(t)\rangle$ is assumed to be minor due to averaging). Rearranging terms on the r.h.s. of Eq. (22), recalling independence





AMTD
3, 2535–2577, 2010



of $n_q$ and $n_0$ on each other and on DSD-related errors, we get

$$\hat{\sigma}^2\left[\langle R_L(t)\rangle|\Omega\right] \cong \left\langle \hat{\sigma}^2_{\mathrm{DSD+Wet}}\left(R_L\left|\hat{A}_R(t)\right.\right)\right\rangle + \frac{1}{\Delta t}\left\langle d_M(t)^2\right\rangle \frac{\Delta^2}{12} + \langle d_M(t)\rangle^2 \hat{\sigma}^2_0. \quad (23)$$

### 2.6 Summary of the uncertainty model

To sum up, we have derived the estimates of path-integrated rainfall-induced attenuation $\hat{A}_R$ and path-averaged rainfall $\hat{R}_L$ in Eqs. (17), (20) based on the model for the measured signal $A_M$ given by Eq. (2), comprising baseline attenuation $A_0$, path-integrated rainfall-induced attenuation $A_R$, wet antenna attenuation $A_w$ and quantization error $n_q$. Using the first-order approximations of nonlinear models for $A_w$ (Eq. 8) and the power-law relation (Eq. 1), the estimate $\hat{A}_R$ in Eq. (17) is equivalent to the deterministic relation (e.g. Leijnse et al., 2007b; Zinevich et al., 2009). Next, we have derived the Eq. (21) for MSE for path-average rainfall estimates, based on an ad hoc model for uncertainty of the $A-R$ relation given by Eq. (11), sample MSE estimate $\hat{\sigma}^2_{0\pm}$ of baseline uncertainty and a simplified model for variance of quantization error (Eq. 3). Finally, Eq. (23) for MSE of time- and path-averaged rainfall has been derived.

## 3 Calibration of model parameters

The model parameters (rainfall attenuation and MSE model coefficients, wet attenuation coefficients) have been calibrated using a DSD database and a set of rain gauge and microwave links records.

The wet antenna attenuation coefficients have been derived from observations of three intensive convective rainstorms (Table 1) recorded in central Israel during the winters 2006, 2007 and 2008 by a commercial network of 23 vertically polarized microwave links, operating at frequencies 17–23 GHz with lengths varying from 0.81 to 7.26 km. The links record quantized instantaneous microwave attenuation with $\Delta = 1$ dB magnitude and one minute temporal resolution. For comparison, five rain gauges,





AMTD
3, 2535–2577, 2010



recording point rain rate with 6 mm $h^{-1}$ magnitude and one minute temporal resolution, have been installed in the vicinity of microwave links (Fig. 2).

The rest of parameters have been derived using the DSD database consisting of 6282 DSD spectra, collected in central Israel during 1984–1985 (courtesy of Z. Levin; see Feingold and Levin, 1986, for details) at the temporal resolution of one minute.

### 3.1 Derivation of power law coefficients

To transform the DSD time series into spatial profiles knowing the rainstorm advection velocity, the Taylor's hypothesis of frozen turbulence is invoked (Leijnse et al., 2008a). As a result, the integration of the space-varying $N_d(D,x)$ along the link can be replaced by integration of discrete point-scale DSD time series

$$\bar{N}_d(D) = \int_0^L N_d(D,x)\,dx \cong \frac{L}{[L/v]} \sum_{t=1}^{[L/v]} N_d(D,t), \tag{24}$$

where $[\cdot]$ stands here for rounding operation, $v$ is the rainstorm advection velocity that has been estimated by correlating multiple microwave links (Zinevich et al., 2009); the (climatological) average for three studied rainstorms (see Table 1) is $v = 14.6\ \mathrm{m\,s^{-1}}$.

The parameters $\alpha$, $\beta$ in Eq. (6) have been obtained using a non-linear fit of $N_R$=6200 DSD profiles $\bar{N}_d(D)$, using the T-matrix method for extinction cross-section (Mishchenko, 2000):

$$[\alpha,\beta] = \underset{\alpha,\beta}{\operatorname{argmin}} \sum_{i=1}^{N_R} \left( R_L(i) - \hat{R}_L(A_R(i)) \right)^2, \tag{25}$$

where $A_R$, $R_L$ and $\hat{R}_L$ are given by Eqs. (4), (5) and (6). The problem in Eq. (25) and the rest of non-linear minimization problems in this study are solved using simplex optimization (Press et al., 1992); preliminary coarse grid search has been done to find optimal initial values, likely leading to a global minimum.





AMTD
3, 2535–2577, 2010



Dealing with disdrometer records requires addressing the sampling error issue; it was shown by Uijlenhoet et al. (2006) that the sampling distribution of any DSD moment converges asymptotically to Gaussian with increase of sample size. The sampling distribution of high moments such as rain rate remains skewed for sample size as large as 500 samples, which results in biased estimates of bulk rainfall variables. In the DSD records used in this study, a typical DSD sample size is a few thousand drops for point rain rates of above 1 mm $h^{-1}$ at one minute resolution. For this reason, the effect of the sampling errors on power-law coefficients is assumed to be negligible.

### 3.2 Derivation of wet antenna attenuation coefficients

It has been shown by Leijnse et al. (2008a) that wet antenna attenuation is essentially independent on frequency at 17–23 GHz, so in this study only link length dependence has been assumed for $c_1$,$c_2$ (i.e. different coefficients for link length ranges 0...1 km, 1...2 km, etc.). Assuming that nearby gauge rainfall records $\langle R_0 \rangle$ averaged over $\Delta t$ minutes approximate averaged link rainfall $\langle R_L \rangle$, the coefficients $c_1$, $c_2$ are

$$c_1, c_2 = \operatorname{argmin} \sum_i \left( \langle R_0 \rangle_i - \left\langle \hat{R}_L \left( \hat{A}_R \right) \right\rangle_i \right)^2, \tag{26}$$

$$\langle \cdot \rangle_i = \sum_{j=i}^{i+\Delta t-1} (\cdot)_j / \Delta t, \tag{27}$$

where $\hat{A}_R$, $\hat{R}_L\left(\hat{A}_R\right)$ are given by Eqs. (17) and (19); averaging $\langle \cdot \rangle_i$ lowers differences due to link-gauge physical separation. Summation through $i$ goes over all available data (Table 1). In practice, estimates of $c_1$, $c_2$ are reliable at $\Delta t \geq 10$ min (i.e. $c_1$, $c_2$ change weakly with further increase of $\Delta t$). Assuming that the sample mean (summation in Eq. 26) approximates the expectation operator, the estimate of $\hat{R}_L(A_R)$ is unbiased (Papoulis, 1991, p. 175); the bias caused by $n_w$ in Eq. (12) is absorbed into the coefficients $c_1$,$c_2$.





AMTD
3, 2535–2577, 2010



### 3.3 Derivation of coefficients of path-averaged rainfall MSE model

Firstly, for each of $N_R$ path-integrated DSD profiles $\bar{N}_d(D)$, calculated according to Eq. (24) from the available DSD data, the path-integrated attenuation $A_R$ is computed using Eq. (4). The instantaneous DSD spectra, multiplied by link length $L \cdot N_d(D,1)$ and $L \cdot N_d\left(D,[L/v]\right)$ at two ends of each profile are substituted into Eq. (4) to calculate path-integrated attenuation values $A_R(j)$, $j$ =1,2, simulating constant DSD along the link. Then, the wet antenna attenuations for two antennas $A_w(j)$, $j$ =1,2 are obtained by solving

$$A_w(j) = a_w(A_R(j) + A_w(j)). \quad (28)$$

Equation (28) is inverted for unknown $A_w(j)$ by golden section search; the value $A_w = (A_w(1) + A_w(2))/2$ is the simulated wet antenna attenuation. Finally, the path-integrated $\hat{A}_R(i)$ is calculated from the full $i$-th DSD profile as

$$\hat{A}_R(i) = A_R + A_w - a_w(A_R + A_w). \quad (29)$$

The above estimation is valid under the assumption that $a_w$ with $c_1$, $c_2$ calibrated using Eq. (26) is applicable for the case of constant DSD along the link. With real data, this assumption, in general, does not hold due to non-linearity of $a_w$:

$$E\left[A_w - a_w(A_R + A_w)|A_w\right] \neq 0. \quad (30)$$

The bias increases with link length and rain rate. Over the available DSD data, the average bias ($\hat{A}_R$ underestimates true $A_R$) is about 5% of $A_R$ (maximum 10% for high rain rates) for links shorter than 3 km (two thirds of the studied data) and reaches 7% (maximum 17%) for 7.16 km links as rainfall variability along the link increases. These results suggest dependence of parameters of the Eq. (8) on rainfall spatial variability; the model, given by Eqs. (28), (29) is better suited for stratiform, homogeneous rainfall, or short links. The optimal wet attenuation coefficients (i.e. producing least biased estimates of rainfall) may therefore be different for different types of rainfall (e.g. convective





AMTD
3, 2535–2577, 2010



or stratiform). In general, a more accurate model for wet antenna is needed (e.g. Leijnse et al., 2008a). The latter, however, requires calibration with gauges, installed at both antenna locations for each link that are unavailable. Equations (28), (29) has been used in the present study despite biasedness, assuming that they still allow estimating the typical scale of wet antenna-related errors.

Next, $\hat{R}_L\left(\hat{A}_{\mathrm{R}}(i)\right)$, $i=1\ldots N_{\mathrm{R}}$ are calculated for all DSD profiles using Eq. (25), and the parameters of the model for MSE of DSD-related uncertatinties are calibrated as

$$[\gamma,\delta,\varepsilon]=\underset{\gamma,\delta,\varepsilon}{\operatorname{argmin}}\sum_{i=1}^{N_{\mathrm{R}}}\left(\left(R_L(i)-\hat{R}_L\left(\hat{A}_{\mathrm{R}}(i)\right)\right)^2-\hat{\sigma}^2_{\mathrm{DSD+Wet}}\left(R_L\left|\hat{A}_{\mathrm{R}}(i)\right.\right)\right)^2. \quad (31)$$

The $i$-th samples $R_L(i)$ and $\hat{R}_L(i)$ are given by Eqs. (5), (6). Examples of $\hat{R}_L\left(\hat{A}_{\mathrm{R}}\right)$ and $\hat{\sigma}_{\mathrm{DSD+Wet}}\left(R_L\left|\hat{A}_{\mathrm{R}}\right.\right)$ are shown in Figs. 3, 4. RMSE increases substantially with link length, due to increased variability between antenna locations. Conversely, excluding wet antenna-related variability from consideration (using Eq. 7 instead of Eq. 11) leads to decrease of MSE for longer links (not shown here); for instantaneous measurements, wet antenna effects mostly dominate the effect of DSD variability along a link. Increasing frequency directly leads to accuracy improvement; thus, 18 GHz link is almost twice more uncertain than 24 GHz one (Fig. 4, right). These results are in agreement with conclusions of Atlas and Ulbrich (1977), Leijnse et al. (2008a).

To assess the accuracy of the approximation of $\hat{\sigma}^2_{\mathrm{DSD+Wet}}$ by Eq. (11), the statistics

$$S_{\mathrm{DSD+Wet}}=\sqrt{\frac{\sum_{i=1}^{N_{\mathrm{R}}}\hat{\sigma}^2_{\mathrm{DSD+Wet}}\left(R_L(i)\left|\hat{A}_{\mathrm{R}}(i)\right.\right)}{\sum_{i=1}^{N_{\mathrm{R}}}\left(R_L(i)-\hat{R}_L\left(\hat{A}_{\mathrm{R}}(i)\right)\right)^2}}. \quad (32)$$





AMTD
3, 2535–2577, 2010



has been calculated for various frequencies 16...38 GHz and link length 0.5...8 km. Values $S_{\mathrm{DSD+Wet}}$ close to one indicate validity of Eq. (11). One can see that in most cases, the error does not exceed few percents, with maximum of 14 percent (Table 2).

The model for $\hat{\sigma}^2_{\mathrm{DSD}}$ (Eq. 7) can be verified similarly to Eq. (11) using statistics in Eq. (32), producing results, similar to ones in Table 2.

In the case of temporal averaging, the coefficients $\gamma$, $\delta$, $\varepsilon$ differ from ones in Eq. (11) as they are calibrated over time-averaged data to take into account correlation between adjacent time frames

$$[\gamma,\delta,\varepsilon] = \underset{\gamma,\delta,\varepsilon}{\operatorname{argmin}} \sum_{i=1}^{N_{\mathrm{R}}} \left( \left( \langle R_L \rangle_i - \left\langle \hat{R}_L \right\rangle_i \right)^2 - \left\langle \hat{\sigma}^2_{\mathrm{DSD+Wet}} \left( R_L \left| \hat{A}_{\mathrm{R}} \right. \right) \right\rangle_i \right)^2 \tag{33}$$

where $\langle \cdot \rangle_i$ is given by Eq. (27). Accuracy of the model for $\Delta t = 1$ and 30 min is comparable.

## 4 Estimation of point rainfall from path-averaged measurements

To compare path-averaged rainfall with the point scale rain gauges, one can address modeling of rainfall spatial variability through the use of geostatistics methods (Schabenberger and Gotway, 2005) to obtain an MSE expression for rainfall estimation at an arbitrary point in space.

### 4.1 Semivariogram modeling

Under the assumption of stationarity of a two-dimensional rainfall field and its isotropy (covariance between rainfall at two points depends only on distance between them), an empirical semivariogram $\gamma(h)$ describes the spatial correlation of rainfall $r$ between two points, separated by distance $h$

$$2\gamma(h) = E\left[ \left( r_{\boldsymbol{x}} - r_{\boldsymbol{x}(h)} \right)^2 \right], \tag{34}$$





AMTD
3, 2535–2577, 2010



where $\boldsymbol{x}(h) = \{\boldsymbol{x}' : \|\boldsymbol{x} - \boldsymbol{x}'\| = h\}$. In practice, an empirical semivariogram $\gamma_E(h)$ is firstly calculated from rainfall data by replacing the expectation operator in Eq. (34) by sample mean and then is approximated by Gaussian semivariogram model (subjectively chosen as it fits Eq. (34) best)

$$\gamma_M(h) = (s-n)\left(1 - \exp\left(-\frac{h^2}{r^2}\right)\right) + n. \quad (35)$$

where sill $s$, nugget $n$ and range $r$ are estimated by non-linear least square fit.

Equation (35) does not assume any a-priori information except for climatologically averaged positive spatial autocorrelation that decreases with distance; in particular, it does not distinguish between weak and strong rainfall. To take this into account, let us assume that the path-averaged rainfall $R_L$ represents the local areal average rainfall in the vicinity of a link (e.g. over a circular area with diameter equal to the link length). Consequently, one can consider an optimal estimate of $\gamma(h)$ given $R_L$. The conditional semivariogram is defined as

$$2\gamma\left(h|R_L\right) = E\left[\left(r_{\boldsymbol{x}} - r_{\boldsymbol{x}(h)}\right)^2 | R_L\right]. \quad (36)$$

Modeling of $\gamma\left(h|R_L\right)$ has been done in two steps. Firstly, empirical conditional semivariograms have been calculated over a series of $N_q$ rainfall intensity ranges $\{q_i\}_{i=1,\ldots,N_q} = \left\{[0,\ldots,p^0),\ldots,[p^{i-2},\ldots,p^{i-1}),\ldots\right\}$ as

$$2\gamma_E\left(h|q_i\right) = \left\langle \left(r_{\boldsymbol{x}_1} - r_{\boldsymbol{x}_2}\right)^2 | h, R_L \right\rangle, \quad (37)$$

where $\langle\cdot\rangle$ denotes averaging over all possible $\{\boldsymbol{x}_1, \boldsymbol{x}_2 : \|\boldsymbol{x}_1 - \boldsymbol{x}_2\| = h,\ R_L(\boldsymbol{x}_1, \boldsymbol{x}_2) \in q_i\}$, $R_L(\boldsymbol{x}_1, \boldsymbol{x}_2)$ is the local areal average rainfall intensity in the vicinity of $\boldsymbol{x}_1, \boldsymbol{x}_2$. The parameter $p$=1.5 has been chosen to maximize $N_q$ provided that no rainfall bins $q_i$ are empty, given the available rain gauge data. The average rainfall estimate $\left(r_{\boldsymbol{x}_1} + r_{\boldsymbol{x}_2}\right)/2$





AMTD
3, 2535–2577, 2010



is substituted for unknown $R_L(\boldsymbol{x}_1,\boldsymbol{x}_2)$. Then, the models $\gamma_M\left(h|\bar{R}_L(i)\right)$, $i=1\ldots N_q$ have been fitted with these empirical semivariograms, producing a set of parameters $\Lambda_i=\{s_i,n_i,r_i\}$, $i=1...N_q$

$$\Lambda_i=\arg\min\sum_h\left(\gamma_E\left(h|q_i\right)^{1/2}-\gamma_M\left(h|\bar{R}_L(i)\right)^{1/2}\right)^2, \quad (38)$$

where average $\bar{R}_L(i)=\langle R_L(\boldsymbol{x}_1,\boldsymbol{x}_2)\in q_i\rangle$. Taking square root of semivariograms in Eq. (38) is necessary to give more weight to small $h$ (small $\gamma$) with respect to large $h$ (considerably larger values of $\gamma$) in numerical optimization.

The empirical semivariograms have been calculated at three different $h$ (1.47, 6.1 and 11 km) from the records of four rain gauges over three rainstorms (Fig. 2 and Table 1). Special attention has been given to the values of $\gamma_E\left(h=0|R_L\right)$ that are crucial for stability of optimization in Eq. (38) but there is no field data available. Considerable differences of rain rate due to spatial variability appear already at $h$=0.4 km, for 0.81 km link L7 and Switch Ramle gauge (Sect. 5), that should be modeled by a non-zero nugget. To force the non-zero nugget in Eq. (35), it has been set $\gamma_E\left(h=0|R_L\right)=\gamma_E\left(h=1.47|R_L\right)$. An example of semivariogram model $\gamma_M\left(h|R_L\right)$ for 10 min average is drawn in Fig. 5 (simulating temporal averaging is straightforward). Note that $\gamma_E$ for $R_L$=19.9 mm h$^{-1}$ exhibits decrease at $h$=11 km that violates an assumption behind the non-decreasing model in Eq. (35); this is attributed to limited amount of available high-intensity data for modeling. As a result, multiple peaks, appearing in a specific event (December 2006, Table 1) express in the model. The values of $\gamma_M\left(h|R_L\right)$ for $R_L$ different from $\bar{R}_L(i)$, $i=1...N_q$ are obtained by linear interpolation of the family $\gamma_M\left(h|\bar{R}_L(i)\right)$, and for $R_L>\bar{R}_L\left(N_q\right)$ by means of linear extrapolation.

### 4.2 Spatial discretization of a microwave link

Representation of a link in a discrete form is done by dividing it into a set of $N$ short intervals where the rainfall intensity is assumed to be constant; the length of an interval





AMTD
3, 2535–2577, 2010



is chosen 0.5 km (Goldshtein et al., 2009). The measured path-averaged rainfall in this model is approximated by averaging point rain rates $R(\boldsymbol{x}_i)$, $i=1,..,N$

$$R_L = \alpha\left(a\int R(\boldsymbol{x})^b d\boldsymbol{x}\right)^{\beta} \cong \frac{1}{N}\sum_{i=1}^{N_w} R(\boldsymbol{x}_i) \tag{39}$$

where the power law coefficients $a$, $b$, $\alpha$, $\beta$ are taken from Eqs. (1) and (6); the integration is done over all points $x$ along the link. The deviation of $R_L$ from the true path-averaged rainfall for $b \neq 1$ is about a few percents (Atlas and Ulbrich, 1977) and is neglected for MSE estimation.

### 4.3 MSE of rainfall estimation

A trivial estimator of the rainfall at the point $\boldsymbol{x}_0$ from a nearby link's measurement is the link's path-averaged rainfall itself, $\hat{R}(\boldsymbol{x}_0) = \hat{R}_L\left(\hat{A}_R\right)$. The MSE expression for the estimate of $R(\boldsymbol{x}_0)$ is

$$\hat{\sigma}^2\left[R(\boldsymbol{x}_0)\middle|\hat{A}_R\right] = E\left[\left(R(\boldsymbol{x}_0) - \hat{R}_L\left(\hat{A}_R\right)\right)^2\right]. \tag{40}$$

By denoting the error in estimation of path-averaged rainfall $e = R_L - \hat{R}_L\left(\hat{A}_R\right)$, substituting Eq. (39) into Eq. (40) and denoting $h_{ij} = \left\|\boldsymbol{x}_i - \boldsymbol{x}_j\right\|$, $i,j=0...N$, Eq. (40) transforms into

$$\sigma^2\left[R(\boldsymbol{x}_0)\middle|\hat{A}_R\right] \cong C(0) + \frac{1}{N^2}\sum_{i=1}^{N}\sum_{j=1}^{N} C\left(h_{ij}\right) - \frac{2}{N}\sum_{i=1}^{N} C(h_{io}) + 2E\left[(R_L - R(\boldsymbol{x}_0))e\middle|\hat{A}_R\right] + E\left[e^2\right]. \tag{41}$$

Here $C\left(h_{ij}\right)$ is a covariance function

$$C\left(h_{ij}\right) = E\left[R(\boldsymbol{x}_i)R\left(\boldsymbol{x}_j\right)\right] - \eta_i\eta_j \tag{42}$$





AMTD
3, 2535–2577, 2010



and $C(0) = \sigma_R^2$ is an a-priori climatological variance of rainfall intensities, under an assumption of constant expected value of rainfall intensity $\eta_i = \eta_j \equiv \eta \forall \boldsymbol{x}_i, \boldsymbol{x}_j$ in the area.

The term $2E\left[(R_L - R(\boldsymbol{x}_0))e \middle| \hat{A}_R\right]$ in Eq. (41) describes covariance between $e$ and local rainfall variation $R_L - R(\boldsymbol{x}_0)$. While the former is mostly measurement error, the latter is due to difference between path-averaged rainfall and rainfall intensity at a single location $\boldsymbol{x}_0$. This term can be neglected under the assumption of independence of $e$ and $R_L - R(\boldsymbol{x}_0)$ ($E[e]$ can be assumed zero according to Eq. 26). However, some components of $e$ (mostly, the errors, related to wet antenna attenuation) do depend on local rainfall variation. Numerical simulation of Eq. (41) using the DSD database (Sect. 3) shows that neglecting $2E\left[(R_L - R(\boldsymbol{x}_0))e \middle| \hat{A}_R\right]$ in Eq. (41) may lead to errors in $\sigma^2\left[R(\boldsymbol{x}_0) \middle| \hat{A}_R\right]$, depending on $\boldsymbol{x}_0$. Thus, locating $\boldsymbol{x}_0$ near one of the antennas leads to overestimation of $\sigma^2\left[R(\boldsymbol{x}_0) \middle| \hat{A}_R\right]$ by up to 12% at $\Delta t$=1 min for long (7.16 km links) L22, L23, since the wet antenna-related errors become more severe for longer links; locating $\boldsymbol{x}_0$ in the middle of a long link leads to underestimation of $\sigma^2\left[R(\boldsymbol{x}_0) \middle| \hat{A}_R\right]$ by up to 15% (the correlation between $e$ and $R_L - R(\boldsymbol{x}_0)$ is negative in this case). The maximum error, introduced by dropping the term $2E\left[(R_L - R(\boldsymbol{x}_0))e \middle| \hat{A}_R\right]$, becomes negligible (about 2% on the average, maximum 4%) for $\Delta t$ above 30 min, for all links besides L22, L23.

The calculation of $E\left[(R_L - R(\boldsymbol{x}_0))e \middle| \hat{A}_R\right]$ is complicated since the models of $R_L - R(\boldsymbol{x}_0)$ and $e$ are calibrated using different datasets – the point gauge records (Table 1) and the DSD database (Sect. 3), respectively; the dependence of $E\left[(R_L - R(\boldsymbol{x}_0))e \middle| \hat{A}_R\right]$ on $\boldsymbol{x}_0$ requires development of an additional model. In this study, we neglect this covariance term, keeping in mind the consequences – overestimation of $\sigma^2\left[R(\boldsymbol{x}_0) \middle| \hat{A}_R\right]$ at short temporal averaging intervals ($\Delta t$ less than 30 min) and for long links L22, L23.





AMTD
3, 2535–2577, 2010



Substituting into Eq. (41)

$$C\left(h_{ij}\right) = C(0) - \gamma\left(h_{ij}\right) \tag{43}$$

and Eq. (11) for $E\left[e^2\right]$, we get the MSE expression in terms of semivariogram

$$\sigma^2\left[R(\boldsymbol{x}_0)\,\middle|\,\hat{A}_{\mathrm{R}}\right] \cong \frac{2}{N}\sum_{i=1}^{N}\gamma(h_{i0}) - \frac{1}{N^2}\sum_{i=1}^{N}\sum_{j=1}^{N}\gamma\left(h_{ij}\right) + \sigma^2_{\mathrm{DSD+Wet}}\left[R_L\,\middle|\,\hat{A}_{\mathrm{R}}\right]. \tag{44}$$

In the case of the conditional semivariogram, $\gamma\left(h|R_0\right)$ is directly substituted into Eq. (44) instead of $\gamma(h)$; this can be done since the condition

$$C\left(h_{ij}|R_0\right) = C\left(0|R_0\right) - \gamma\left(h_{ij}|R_0\right) \tag{45}$$

holds under the assumption of constant mean rainfall $R_0$ in the vicinity of the link, i.e. $E\left[R\left(\boldsymbol{x}_j\right)|R_0\right] = E\left[R(\boldsymbol{x}_i)|R_0\right] = R_0$ for all pairs of $i, j = 0 \ldots N$.

## 5 Results and discussion

Performance of the uncertainty quantification models have been evaluated using records of 63 link-gauge pairs (Sect. 3, Fig. 2) over three convective rainstorms (Table 1). The statistics $S_j$ for the accuracy of MSE prediction $p_j$ (Xu and Wilke, 2005) with respect to measured error $e_j$ ($j = 1 \ldots 63$) are

$$e_j = \sqrt{\frac{1}{T_j}\sum_{t=1}^{T_j}\left(R(t,j) - \hat{R}(t,j)\right)^2}, \quad p_j = \sqrt{\frac{1}{T_j}\sum_{t=1}^{T_j}\hat{\sigma}^2_{tj}}, \quad S_j = p_j / e_j, \tag{46}$$

where $t = 1 \ldots T_j$ is the index of a sample (averaging over $\Delta t$ minute interval) for the $j$-th link-gauge pair, $R(t,j)$ and $\hat{R}(t,j)$ are the gauge measurement and link estimate at time





AMTD
3, 2535–2577, 2010



$t$, and $\hat{\sigma}^2_{tj}$ is the predicted MSE, given by Eq. (44). The values of $S_j$ close to one indicate correct prediction of measurement errors. To examine relative role of each one of the error sources, the results have been calculated at various temporal averaging intervals ($\Delta t$=1, 5, 10, 15, 30, 60 and 120 min).

To get insight into the respective contribution of each component of the measured attenuation model into the predicted error, statistics in Eq. (46) have been computed excluding some error sources (i.e. zeroing their respective MSE estimates in Eq. 44):

1. *Spatial+Link* – prediction of the total error, including all error sources.
2. *Spatial* – prediction of error due to spatial rainfall variability only.
3. *DSD* – prediction of error due to DSD variability along the link only.
4. *Wet* – prediction of error due to antenna wetting only.
5. *Quant* – prediction of quantization error only.
6. *Baseline* – prediction of baseline-related errors only.

An example time series of the measured error $e_j$ vs. predicted RMSE $p_j$ for 10-min average rainfall is shown in Fig. 6, bottom. For clarity, the results are presented in the form of measured and predicted RMSE of accumulated rainfall estimates. One can see that at about 13:30 LT 4 January 2008 the link overestimates rainfall with respect to Switch Ramle rain gauge, while at about 18:30 the gauge records a strong peak, missed by the link (Fig. 6, top). As a result, the error prediction *Spatial+Link*, based on the link measurements and closely following the measured error until 13:30, overestimates measurement error between 13:30 and 18:30 and underestimates starting from about 18:30 (Fig. 6, bottom). This shows that even at short spatial distance (link length 0.81 km and the link-gauge distance is 0.45 km), spatial rainfall variability strongly affects the error prediction accuracy, and even a single peak may cause considerable measurement errors.





AMTD
3, 2535–2577, 2010



Taking into account this dominating effect of spatial variability and simplifying assumptions made in Sect. 4 (e.g. inferring local areal-average rainfall from link measurements, semivariogram modeling with gauge records), one should expect that the error predictions should be correct only on the average. The total statistics $\bar{S}$ are used to estimate the accuracy of MSE prediction:

$$\bar{e} = \sqrt{\sum_{j\in J}\sum_{t=1}^{T_j} \hat{\sigma}_{tj}^2}, \quad \bar{p} = \sqrt{\sum_{j\in J}\sum_{t=1}^{T_j} \left(R(t,j) - \hat{R}(t,j)\right)^2}, \quad \bar{S} = \bar{p}/\bar{e} \tag{47}$$

where $J$ is a chosen subset of link-gauge pairs to represent a specific interval of link lengths or rain rates.

### 5.1 Accuracy of error predictions at various temporal resolutions

Figure 7 shows the performance statistics $\bar{S}$ for various error sources at different temporal resolutions (accumulation intervals) $\Delta t$. At all temporal averaging intervals, spatial variability uncertainty dominates the link-related uncertainties (Fig. 7, bottom), even though the role of the latter increases with $\Delta t$. The baseline uncertainty is the major error source among link-related ones. The predicted wet antenna-related errors decrease with increasing $\Delta t$: $\bar{p}$(Wet) changes from 0.37 mm h$^{-1}$ at one minute resolution up to 0.09 mm h$^{-1}$ at 120 min (Fig. 7, bottom). The predicted quantization errors, independent for different observations, also lower with increasing $\Delta t$ (from 0.32 to 0.03 mm h$^{-1}$). The DSD-related errors $\bar{p}$(DSD) exhibit similar dependence, but to less extent (from 0.26 to 0.07 mm h$^{-1}$), due to inter-storm variability in the DSD.

The statistics $\bar{S}$ varies with $\Delta t$ from 1.01 to 0.88 (Fig. 7, top) that shows more accurate error prediction than it has been reported in the literature (the simulation by Leijnse et al. (2008a) has allowed prediction of 32% normalized RMSE vs. 94% measured one, that equals $\bar{S}$=0.34), due to inclusion of uncertainties, related to the difference in link-gauge physical locations and baseline estimation uncertainty.





AMTD
3, 2535–2577, 2010



Note that the semivariograms, calculated from the records of two point rain gauges, absorb 6 mm h$^{-1}$ quantization rain gauges errors twice, while in link-gauge comparison it presents only once, that may contribute into error overestimation at $\Delta t$=1 min; for longer $\Delta t$, this effect quickly diminishes (only amount of water in a bucket before and after the accumulation interval is uncertain). For most link-gauge pairs, the gauge is located at one of the link ends (Fig. 2); this also leads to overestimation in MSE prediction at short $\Delta t$ (less than 30 min) due to the neglected covariance term in Eq. (41). The approximation of a link by its midpoint (i.e. setting $N_w$ =1 in Eq. 39) results in additional RMSE overestimation: $\bar{S}$ values for various $\Delta t$ lie between 0.98 to 1.12 that confirms necessity of modeling rainfall variability along a link according to Eq. (41).

The scatter plot (Fig. 8, left) shows that the rainfall estimation is overall unbiased (the regression line is close to 1:1). There are three groups of points in the graph, corresponding to three events (Table 1); microwave links slightly overestimate gauges in January 2008 rainstorm (average gauge rainfall of 1.2 mm h$^{-1}$), but underestimate in December, 2006 rainstorm (average gauge rainfall or around 3 mm h$^{-1}$). The December 2006 event is characterized by intense isolated peaks in gauge records that are underestimated by path-averaged links records. The calibration of $\hat{R}_L\left(\hat{A}_R\right)$ according to minimum MSE in Eq. (24) leads to absorbing this discrepancy into the wet attenuation coefficients and affects the entire range of rainfall intensities that, in turn, leads to overestimation of low rain rates and underestimation of high ones. This effect expresses also in the error comparison scatter plot (Fig. 8, right): high measurement errors (around measured RMSE of 2 mm h$^{-1}$) tend to be underestimated. The effect becomes prominent with increase of $\Delta t$ to 120 min, leading to lowering of the regression slope coefficient from 0.76 to 0.52. On the other hand, for $\Delta t$=1–30 min, the slope varies between 0.93...1.30; its deviation from one is mostly due to overestimation by L22, L23, discussed next.





AMTD
3, 2535–2577, 2010



### 5.2 Accuracy of error predictions as a function of link length and rain rate

The dependence of the performance statistics $\bar{S}$ for major error sources as well as measured and predicted errors as a function of link length are shown in the Fig. 9. The spatial variability errors increase with link length; their relative contribution also increases. In most cases, lengths are correlative with link-gauge separation distances (Fig. 4.2), that contributes as well. Quantization and baseline-related errors behave inversely: for longer links, their contribution lowers. The DSD- and wet antenna- related errors increase for longer links for different reasons: wet antenna-related errors naturally grow with link length due to increased spatial variability (Fig. 4, left), while the errors due to DSD variability along the link also grow due to lowering frequency band (from 22 GHz for short links to 18 GHz for 4.21–5.92 km links L4, L11, L13, L27, L17, L24).

The regression line in Fig. 9 (top left) shows a trend of $S_j$ that is partially due to prominent overestimation of the predicted errors for 7.16 km links L22, L23, associated with December 2006. One of the reasons for the overestimation is the neglected covariance term in Eq. (41); another one is the suboptimality of isotropic semivariogram models, discussed next. This rainstorm exhibits a sequence of fronts driven by western winds (Zinevich et al., 2009), in parallel to the links L22, L23 (Fig. 2); the variability of rainfall along the front is much lower than predicted. The empirical semivariograms in Eq. (37) have been calculated at $h$=6 km from the records of Switch Ramle and Kfar Shmuel gauges; the semivariograms therefore model the variability orthogonally to the fronts that is much higher. In this case, the assumption behind the isotropic semivariogram has been violated. On the other hand, the errors are underestimated for 0.81 km links L7, L26, most likely because there is no data available to accurately estimate semivariogram at short gauge separation (that is, non-zero nugget is underestimated in Eq. 35). Excluding links L22, L23, and L7, L26 leads to the regression line close to 1:1.

The dependences of $\bar{S}$, $\bar{e}$ and $\bar{p}$ on average rainfall intensity (as recorded by gauges) are shown in Fig. 10. The contribution of all error sources increases with rain rate,





AMTD
3, 2535–2577, 2010



but the growth of spatial variability errors is most prominent; it is predicted well by conditional semivariogram models (Fig. 10, top left).

## 6 Conclusions

Various error sources affecting accuracy of rain rate estimation using commercial microwave links have been examined, and an analytical expression for MSE of rainfall estimation from attenuation, measured by a single link has been derived. Even though a number of simplifying assumptions have been made (e.g. isotropy of the semivariograms and covariance functions, second-order stationarity of distribution of rainfall intensities in space and time), the experimental errors are mostly in agreement with the predicted ones for various link lengths, rain rates and temporal averaging intervals. The accuracy of the link-gauge error prediction is higher than that reported in the literature (Leijnse et al., 2008a), since additional error sources (baseline variability and spatial rainfall variability) have been taken into account in the proposed model.

The major source of errors in estimating path-averaged rainfall by a link is the baseline uncertainty that dominates other instrumental (quantization error, wet antenna attenuation variability) and environmental (DSD variability along a link) effects. It is known that DSD variability is the major error source in radar backscattering measurements; its effect on forward scattering and absorption measurements by a link is much smaller (Jameson, 1991) and is masked by other error sources. For this reason, the accuracy of prediction of DSD variability-related errors cannot be comprehensively assessed in the presence of other error sources but only based on the point DSD records. Spatial rainfall variability is the primary source of discrepancy between link-gauge measurements, suggesting that effect of spatial variability will remain major in extrapolation of path-averaged observations into areal averages.

The error calculation has been validated over only three convective rainstorms in Israeli climate; studying stratiform and other types of rainfall is desirable as it may reveal a different relative contribution of the error sources. The rest of discrepancies is likely to





AMTD
3, 2535–2577, 2010



arise from modeling errors (e.g. a number of simplifying assumptions have been made for spatial variability modeling) and other unaccounted error sources – for example, effects of natural temperature variations (Leijnse et al., 2007a) and anomalous propagation (ducting). It is assumed that the baseline variation during the rainstorm can be adequately described by pre- and post- rainstorm measurements, while plausibility of this assumption is verified only indirectly. On the other hand, some assumptions (e.g. adequacy of quantization error model in Eq. (3), effect of quantization on accuracy of baseline variance estimation, suboptimality of wet antenna-related error model in Eq. 30) cannot be thoroughly examined in the present setup, since these error sources are minor and are masked by others.

In addition, the presented results are based on an assumption that the wet antenna coefficients and semivariogram models are known perfectly: they have been estimated from link-gauge records over the same events, used subsequently for evaluation. A direct drawback of such approach is overfitting: the wet attenuation coefficients may have absorbed a part of other link-gauge differences (e.g. baseline errors, differences due to spatial variability and errors due to inappropriateness of power law coefficients) that in turn may result in overestimation of error prediction accuracy; it is assumed that these effects are limited because of large amount of calibration data and various link-gauge combinations. It has been shown that the wet attenuation model is not invariant to the differences in spatial rainfall variability that requires further research.

For practical real-time applications, either climatological average or forecasted semivariogram models should be used; the baseline attenuation should also be predicted from past dry estimates, and forecast-related errors should be studied as well. In addition, high temporal resolution measurements are not always available; other temporal sampling strategies lead to additional errors (Leijnse et al., 2008a). The MSE expressions for path-averaged rainfall assume specific climatology (the ad hoc parametric model of $\hat{\sigma}^2_{\mathrm{DSD}}$ in Eq. (7) has been built according to Israeli DSD data).

The MSE expressions for path-integrated rainfall measurements can further be used in data assimilation algorithms (e.g. Grum et al., 2005; Zinevich et al., 2009) as





AMTD
3, 2535–2577, 2010



variance estimates (it has been shown that the biases of rainfall estimation are very limited), providing means for weighing observations according to their uncertainty. Similarly, since spatial variability is a major error source, its modeling is essential for reconstruction of spatial rainfall distribution from multiple links. The isotropic semivariogram model allows explaining most of the errors; the experimental results suggest that an anisotropic model would allow higher error prediction accuracy for Israeli convective rainstorms.

*Acknowledgements.* The authors deeply thank A. Shilo, E. Moshayov (Pelephone) and A. Rayitsfeld (Tel Aviv University) for their cooperation in supplying microwave data and help in installation of rain gauges. This research was funded by Israel Science Foundation (ISF) and the Porter School of Environmental Studies at Tel Aviv University.

## References

Atlas, D. and Ulbrich, C.: Path- and area-integrated rainfall measurement by microwave attenuation in the 1–3 cm band, J. Appl. Meteorol., 16, 1322–1331, 1977.

Aydin, K. and Daisley, S.: Relationships between rainfall rate and 35-ghz attenuation and differential attenuation: modeling the effects of raindrop size distribution, canting, and oscillation, IEEE T. Geosci. Remote, 40(11), 2343–2352, 2002.

Berne, A. and Uijlenhoet, R.: Path-averaged rainfall estimation using microwave links: Uncertainty due to spatial rainfall variability, Geophys. Res. Lett., 34, L07403, doi:10.1029/2007GRL029409, 2007.

David, N., Alpert, P., and Messer, H.: Technical Note: Novel method for water vapour monitoring using wireless communication networks measurements, Atmos. Chem. Phys., 9, 2413–2418, doi:10.5194/acp-9-2413-2009, 2009.

Feingold, G. and Levin, Z.: The lognormal fit to raindrop spectra from frontal convective clouds in Israel, J. Appl. Meteorol., 25, 1346–1363, 1986.

Goldshtein, O., Messer, H., and Zinevich, A.: Rain rate estimation using measurements from commercial telecommunications links, IEEE T. Signal Proces., 57(4), 1616–1625, 2009.

Grum, M., Kraemer, S., Verworn, H., and Redder, A.: Combined use of point rain gauges,





AMTD
3, 2535–2577, 2010



radar, microwave link and level measurements in urban hydrological modeling, Atmos. Res., 77(1–4), 313–321, 2005.
Holt, A. R., Kuznetsov, G., and Rahimi, A. R.: Comparison of the use of dual-frequency and single-frequency attenuation for the measurement of path-averaged rainfall along a microwave links, IEE P-Microw. Anten. P., 150(5), 315–320, 2003.
Jameson, A.: A comparison of microwave techniques for measuring rainfall, J. Appl. Meteorol., 30, 32–54, 1991.
Kharadly, M. and Ross, R.: Effect of wet antenna attenuation on propagation data statistics, IEEE T. Antenn. Propag., 49(8), 1183–1191, 2001.
Krystek, M. and Anton, M.: A weighted total least-squares algorithm for fitting a straight line, Meas. Sci. Technol., 18, 3438–3442, 2007.
Leijnse, H., Uijlenhoet, R., and Stricker, J.: Rainfall measurement using radio links from cellular communication networks, Water Resour. Res., 43(3), W03201, doi:10.1029/2006WR005631, 2007a.
Leijnse, H., Uijlenhoet, R., and Stricker, J.: Hydrometeorological application of a microwave link: 2. Precipitation, Water Resour. Res., 43, W04417, doi:10.1029/2006WR004989, 2007b.
Leijnse, H., Uijlenhoet, R., and Stricker, J.: Microwave link rainfall estimation: Effects of link length and frequency, temporal sampling, power resolution, and wet antenna attenuation, Adv. Water Resour., 31, 1481–1493, doi:10.1016/j.advwatres.2008.03.004, 2008a.
Leijnse, H., Uijlenhoet, R., and Stricker, J.: Sources of error in microwave link rainfall estimation, Proceedings of the International Symposium on Weather Radar and Hydrology, Grenoble, France, 2008b.
Messer, H., Zinevich, A., and Alpert, P.: Environmental monitoring by microwave communication networks, Science, 312, 713, 2006.
Minda, H. and Nakamura, K.: High temporal resolution path-average rain gauge with 50-GHz band microwave, J. Atmos. Ocean. Tech., 22, 165–179, 2005.
Mishchenko, M.: Calculation of the amplitude matrix for a nonspherical particle in a fixed orientation, Appl. Optics, 39(6), 1026–1031, 2000.
Papoulis, A.: Probability, random variables and stochastic processes, 3rd Ed., McGraw-Hill, Singapore, 1991.
Press, W., Teukolsky, S., Vetterling, W., and Flannery, B.: Numerical recipes in C: the art of scientific computing, 2nd Ed., Cambridge University Press, Cambridge, UK, 1992.
Rahimi, A. R., Holt, A. R., Upton, G. J. G., and Cummings, R. J.: The use of dual-frequency





AMTD
3, 2535–2577, 2010



microwave links for measuring path-averaged rainfall, J. Geophys. Res., 108(D15), ACL 8-1, 2003.
Rincon, R. and Lang, R.: Microwave link dual-wavelength measurements of path average attenuation for the estimation of drop size distributions and rainfall, IEEE T. Geosci. Remote, 40(4), 760–770, 2002.
Schabenberger, O. and Gotway, C.: Statistical methods for spatial data analyses, Chapman & Hall/CRC, Boca Raton, FL, USA, 2005.
Uijlenhoet, R., Porrà, J., Torres, D., and Creutin, J.-D.: Analytical solutions to sampling effects in drop size distribution measurements during stationary rainfall: Estimation of bulk rainfall variables, J. Hydrol., 328, 65–82, doi:10.1016/j.jhydrol.2005.11.043, 2006.
Upton, G. J. G., Cummings, R. J., Rahimi, A. R., and Goddard, J. W. F.: Microwave links: the future of urban rainfall measurement?, Atmos. Res., 77(1–4), 300–312, 2005.
Widrow, B. and Kollár, I.: Quantization noise: roundoff error in digital computation, signal processing, control, and communications, Cambridge University Press, Cambridge, UK, 2008.
Xu, K. and Wilke, C.: A kernel-based spatio-temporal dynamical model for nowcasting weather radar reflectivities, J. Am. Stat. Assoc., 100(472), 1133–1144, 2005.
Zinevich, A., Messer, H., and Alpert, P.: Frontal rainfall observation by a commercial microwave communication network, J. Appl. Meteorol. Clim., 48(7), 1317–1344, doi:10.1175/2008jamc2014.1, 2009.





AMTD
3, 2535–2577, 2010



**Table 1.** List of rainstorms, used for empirical assessment of MSE prediction accuracy.

| Event | Duration, h | Net rainfall duration, h | Peak rain rate, mm $h^{-1}$ | Average rain rate, mm $h^{-1}$ |
|---|---|---|---|---|
| 26 December 2006, 12:00 | 22 | 9.6 | 84 | 2.97 |
| 5 January 2007, 12:15 | 62 | 11.6 | 48 | 0.81 |
| 4 January 2008, 10:30 | 9.5 | 1.9 | 54 | 1.22 |
| Total | 93.5 | 23.1 | | 1.28 |





AMTD
3, 2535–2577, 2010



**Table 2.** The performance statistics $S_{DSD+Wet}$ (Eq. 32) for various rain rates and frequencies.

| $R$, mm h$^{-1}$ | 2 km 16 GHz | 2 km 20 GHz | 2 km 24 GHz | 2 km 38 GHz | 0.5 km 20 GHz | 4 km 20 GHz | 8 km 20 GHz | 8 km 38 GHz |
|---|---|---|---|---|---|---|---|---|
| 1–10 | 0.99 | 0.99 | 1.00 | 1.14 | 1.00 | 0.99 | 1.00 | 0.98 |
| 10–100 | 0.96 | 0.97 | 0.98 | 0.96 | 0.99 | 0.97 | 0.99 | 1.04 |





AMTD
3, 2535–2577, 2010



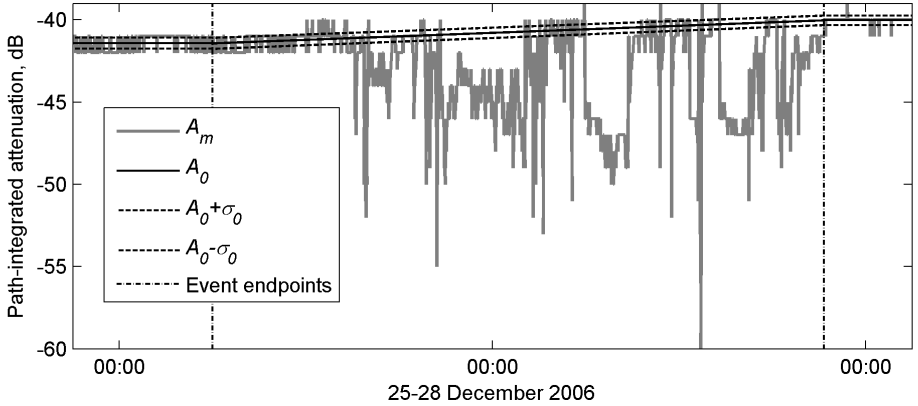


**Fig. 1.** An example of the baseline attenuation determination (23.27 GHz, 2.19 km). $A_M$ is the measured attenuation, $A_0$ is the estimated baseline, and $\sigma_0$ is RMSE of $A_0$. Event endpoints, defining the beginning and the end of the rainstorm, are determined according to the nearby Switch Ramle gauge.





AMTD
3, 2535–2577, 2010



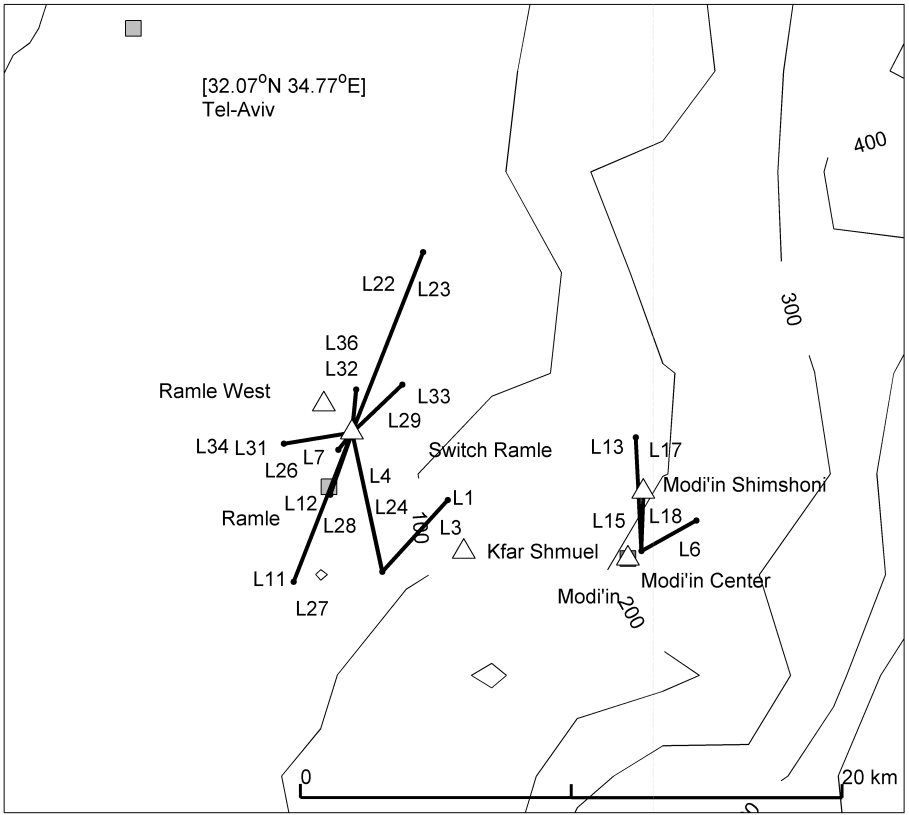


**Fig. 2.** Locations of microwave links, used for rainfall observations, around the cities of Ramle and Modi'in (□) and rain gauges (Δ) Ramle West, Switch Ramle, Kfar Shmuel, Modi'in Shimshoni and Modi'in Center. The local topography contours are given in meters. The duplicating links installed in parallel are denoted twice, e.g. L22 and L23.





AMTD
3, 2535–2577, 2010



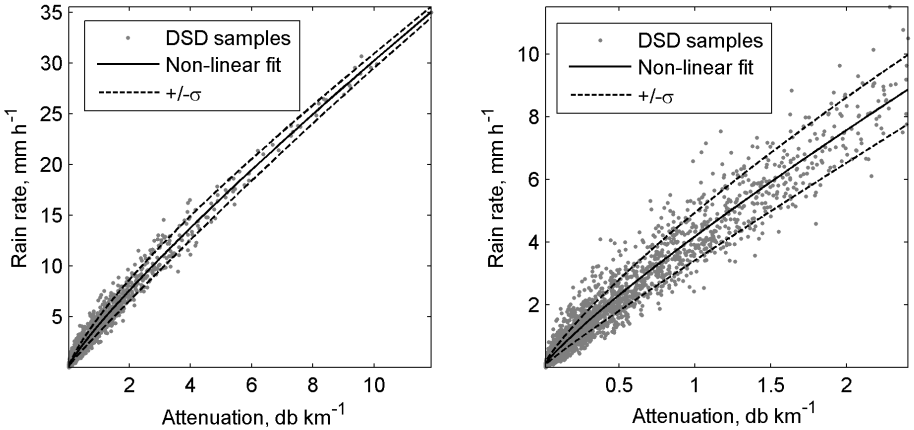


**Fig. 3.** An example of the power-law fit (Eq. 6) and predicted RMSE (Eq. 11) of path-integrated attenuation (Eq. 4) and path-averaged rain rate (Eq. 5) of the DSD database, including variations in DSD and wet antenna attenuation, for a 4 km 20 GHz link. The right figure is a zoomed version of the left one.





AMTD
3, 2535–2577, 2010



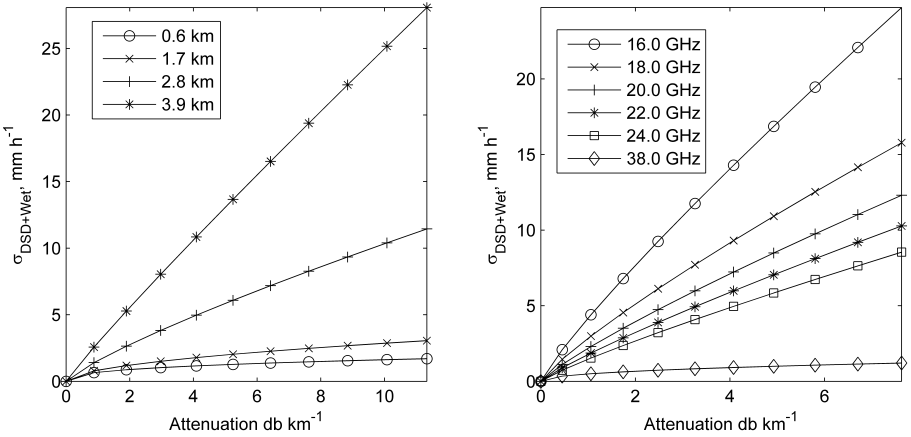


**Fig. 4.** The predicted RMSE of rain rate estimates $\hat{\sigma}_{\mathrm{DSD+Wet}}\left(R_L|A_{\mathrm{R}}+n_{\mathrm{w}}\right)$ (Eq. 11) as a function of link length for a 22 GHz vertically-polarized link (left) and as a function of link frequency for a 2.2 km link (right).





AMTD
3, 2535–2577, 2010



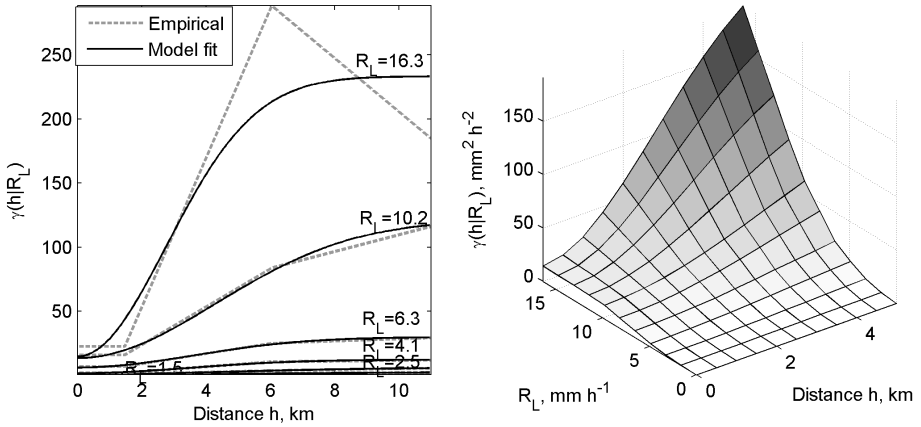


**Fig. 5.** Examples of empirical and model conditional semivariograms for different values of $R_L$ (left) and the resulting three-dimensional function $\gamma\left(h|R_L\right)$ (right), 10 min average.





AMTD
3, 2535–2577, 2010



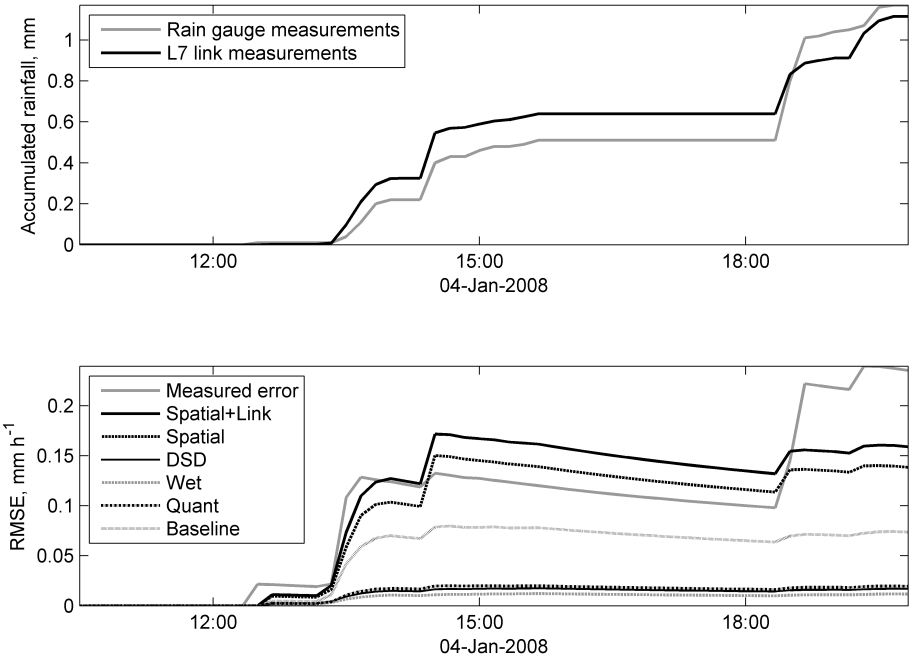


**Fig. 6.** Time series of accumulated gauge rainfall vs. microwave rainfall (upper plot) and measured vs. predicted RMSE (Eq. 46) of accumulated microwave rainfall estimates (lower plot). Contribution of various error sources into the total predicted error is shown in the lower plot, for L7 link and Switch Ramle gauge in January 2008 rainstorm. Link length is 0.81 km, frequency is 23.27 GHz, $\Delta t = 10$ min. Note the different scales of the upper and lower plots.





AMTD
3, 2535–2577, 2010



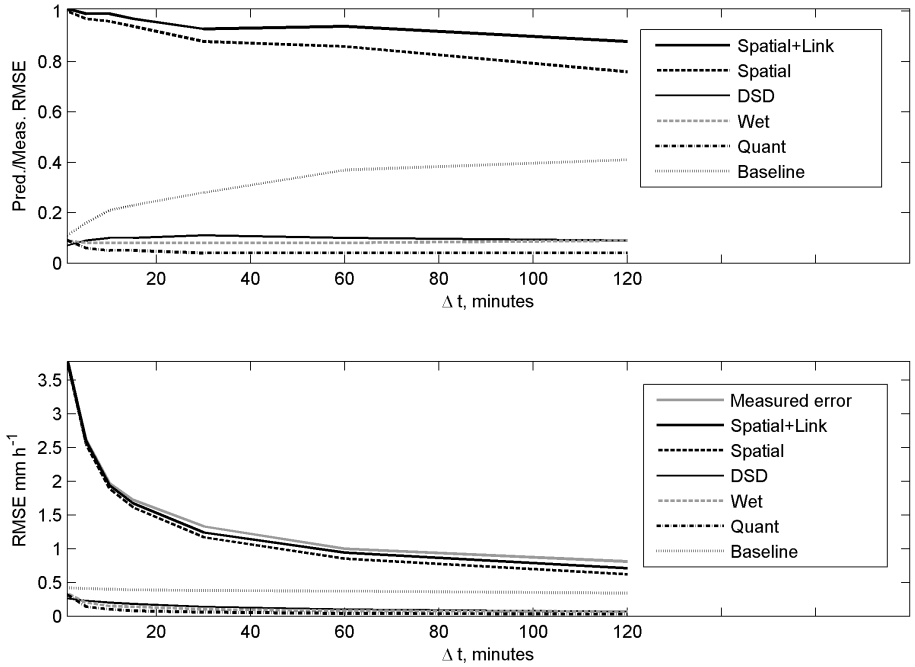


**Fig. 7.** Performance statistics $\bar{S}$ (top), measured $\bar{e}$ and predicted accumulated errors $\bar{p}$ (Eq. 47) for various error sources (bottom), as a function of temporal averaging interval.





AMTD
3, 2535–2577, 2010



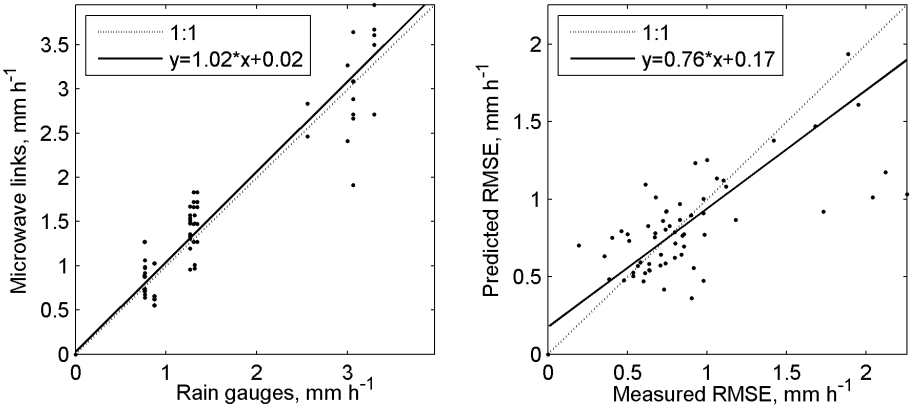


**Fig. 8.** Scatter plots of the total microwave measured rainfall vs. rain gauge measurements (left) and *Spatial+Link* estimates of the prediction error vs. measured error (right) for all link-gauge combinations, $\Delta t = 60$ min. The method of total least squares, assuming uncertainties in both independent and dependent variables (Krystek and Anton, 2007) has been used to draw regression lines.





AMTD
3, 2535–2577, 2010



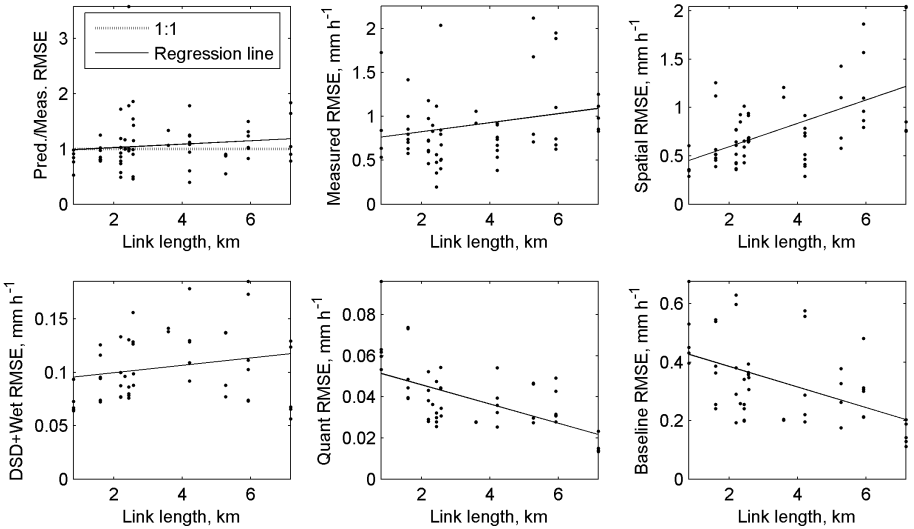


**Fig. 9.** Performance statistics $S_j$, $j$=1,..,63 (Eq. 46) for total predicted error, measured errors and various error sources (spatial variability, DSD and wet antenna, quantization and baseline), as a function of link length, $\Delta t$=60 min.





AMTD
3, 2535–2577, 2010



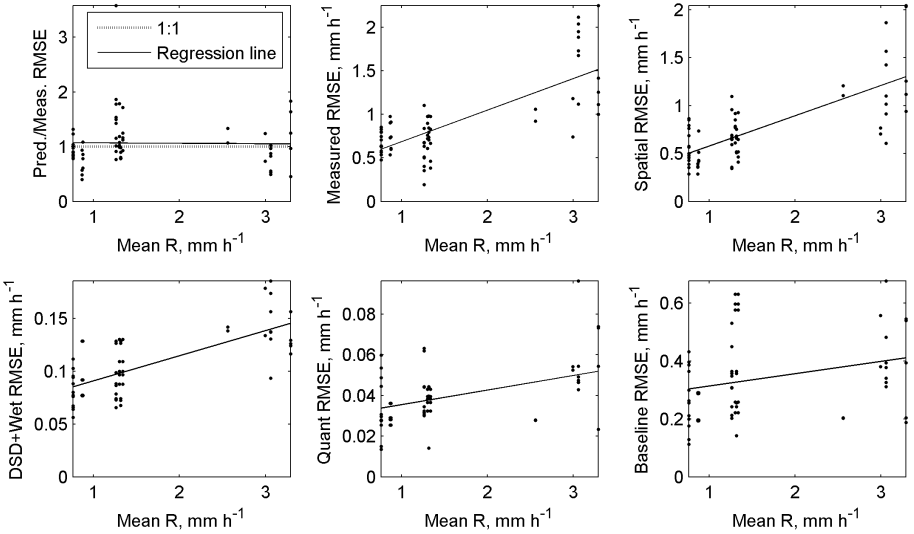


**Fig. 10.** Performance statistics $S_j$, $j$=1,..,63 (Eq. 46) for total predicted error, measured errors and various errors sources (spatial variability, DSD and wet antenna, quantization and baseline), as a function of rain rate recorded by a nearby rain gauge, $\Delta t$=60 min.





AMTD
3, 2535–2577, 2010